2016

The derivation of sea surface velocities from satellite imagery using maximum cross correlation (MCC)

Lawrence, P.

Lawrence, P. (2016) 'The derivation of sea surface velocities from satellite imagery using maximum cross correlation (MCC)', The Plymouth Student Scientist, 9(1), p. 145-161. http://hdl.handle.net/10026.1/14119

The Plymouth Student Scientist
University of Plymouth

*The Plymouth Student Scientist, 2016, **9**, (1), 145-161*

The derivation of sea surface velocities from satellite imagery using maximum cross correlation (MCC)

Philip Lawrence

Project Advisor: Jill Schwarz, School of Marine Science & Engineering, Plymouth University, Drake Circus, Plymouth, PL4 8AA

Abstract

An investigation into the use of cross-correlation statistics to resolve surface velocities from satellite imagery was conducted for the region characterised by the Benguela current at approximately 24^{o}S - 28^{o}S and 9^{o}E - 17^{o}E for July 14th and 15th 2011. Colour images depicting concentrations for chlorophyll_a taken by the MODIS sensor and provided by NASA's Ocean Color Browser, were used to conduct the statistical analysis using distinguishable surface colour features as tracers. Three runs using different parameter values for the cross correlation were carried out and the output vector fields examined. The first run produced 126 vectors with mean *u* and *v* velocities of 10.55 cms^{-1} and 13.37 cms^{-1} respectively. The subsequent run produced 70 vectors with mean velocities of 1.82 cms^{-1} for u and 15.97 cms^{-1} for v. The final run computed 29 vectors showing a mean *u* and *v* velocity of 18.75 cms^{-1} and 12.12 cms^{-1}. These were then compared to velocities derived from ARGO drifter data and probability values for the first, second and third set of distributions calculated. These were 7.03x10^{-7}, 5.26x10^{-4} and 0.0028 respectively (significance level=0.01). The vector positions were compared to those derived using AVISO altimetry data and showed a general agreement regarding circulatory patterns. Limitations such as correlation parameters, temporal and spatial resolutions, data quality and quantity as well as human error may have restricted the success of the method to a certain degree and should be addressed in future implementation.

Introduction

Surface currents

Surface ocean currents have always been of particular interest to oceanographers as they play an important role in forming large scale ocean circulation patterns. These patterns can be used to derive information regarding thermohaline circulation, ocean gyre formation, up or downwelling events, motion of specific water masses, transport of marine organisms or the redistribution of heat in current flows such as the Gulf Stream. As a consequence, quantifying surface currents has long been a priority (Bernstein et al., 1977. Barrick et al., 1977. Bryden & Hall, 1980. Goldstein & Zebker, 1987). Mapping these has proven useful for numerous applications from aiding search and rescue missions, containment of oil, toxic or other polluting chemical spills, economization of ship routes, management of resources and exploitation of living resources (Breaker et al., 1994).

A number of techniques used to measure surface flows exist. Measurement at a local scale is often carried out at fixed positions using either an electro-mechanical current meter or an Acoustic Doppler Current Profiler (ADCP). These Eulerian methods provide accurate *in-situ* results and can quantify current velocities at regular depth and time intervals. Moored devices however are frequently impaired by wave and current action (Breaker et al. 1994). These methods are also time consuming when measuring the flow of a larger, meso-scalar ocean basin (O 100km) thus making it increasingly difficult to resolve surface flows over shorter time periods.

In contrast, Langrangian techniques such as tracked drifters can be used to determine flow on a higher spatial domain. Modern drifters tend to carry a global positioning system (GPS) transmitter to enable the monitoring of coordinates up to ±10 m (Barbanti et al. 2005). The time it takes for a field to evolve, however, can limit the spatial coverage of the drifters (Notarstefano et al. 2007). Similar to Eulerian methods there is also the question of whether the values can be considered to be truly representative of the surface current as drifters will often take near-surface measurements in order to negate direct wind effects on the buoy (Notarstefano et al. 2007).

High Frequency (HF) radar systems can also be used to produce radial current fields from the Doppler shift of the radar signal associated with Bragg lines taken from backscatter data. Determination of current velocities using this method can be highly accurate and averaged to produce hourly maps (Notarstefano et al. 2007). Although the error tends to be minimal, HF radar data is often restricted to 100-200km from the coastal radar station (Paduan & Graber, 1997). This may be useful when investigating the properties of coastal currents but proves less practical when trying to determine the values of off shore ocean currents.

Due to some of the inherent difficulties associated with Eulerian and Langragian tracers, satellite remote sensing has become a more attractive measurement technique with the prospect of saving time and resources while maintaining high quality results over a larger spatial field.

Satellite imagery

Throughout recent years satellite remote sensing has become an attractive tool for monitoring terrestrial features. A growing number of applications implement the use of satellite image analysis within marine related fields. These include the mapping of changes related to ocean surface topography, waves, winds, phytoplankton

concentration, sea ice extension, rainfall, sunlight input, SST among others. The discretisation of light reflected, backscattered or emitted from a body grants the feature a specific 'spectral signature'. Specialised sensors on satellites facilitate the detection of these. However interactions with other bodies such as clouds, the atmosphere or the sensor itself can limit the amount of light detected. Therefore each channel is constrained to sensing light at a certain spatial resolution. The Moderate-resolution Imaging Spectroradiometer (MODIS) on board the Terra and Aqua satellites has channels containing 36 spectral bands ranging from 0.4 μm to 14.4 μm most of these restricted to a spatial resolution of 1km. The temporal resolution of the orbiting satellite will also restrict detection. The MODIS sensor takes 1 to 2 days to cover the Earth meaning the frequency of data acquired for an ocean basin may be restricted to a minimal temporal resolution of ~24h depending also on the sensor design.

Feature tracking

The ability to produce images depicting features such as chlorophyll concentration allows for the tracking of relative motions using an image sequence. The vector velocities can be derived from the associated displacement. This concept works by the identification of a unique feature in two successive, co-registered images, measuring the displacement and then dividing this value by the time interval. i.e. $v = \Delta d/\Delta t$.

This method of tracking, also known as change detection analysis, dates back to the 1950's where tracking was used for military reconnaissance using mounted cameras on stratosphere balloons (Doty, R. 1958). Certain inaccuracies to this technique exist however. The first is the assumption that the feature being tracked serves as a passive tracer that only moves due to horizontal surface advection. This can become problematic as what may seem like a sea surface temperature displacement could in fact be a heating and cooling process or may disappear altogether through diffusion (Emery et al.1991). One way to overcome this problem is to reduce the time separation between images so that most large scale processes can be neglected. Svejkovsky (1988) found that using time separations for Advanced Very High Resolution Radiometer (AVHRR) images of 12-24 hrs produced vector fields with improved accuracy. More recent studies suggest that reducing this parameter further would promote more accurate results (Tokmakian et al.1990).

The calculation of low level winds through selected cloud tracking in meteorology (Leese et al.1971*;* Schmetz and Nuret 1987*)* is one of the first studies to implement feature tracking within the ocean and atmospheric sciences. The technique was then incorporated into aerial photography and was used to illustrate oceanographic patterns (Burgess and James 1971). The use of dyes as a passive tracer has also been used to facilitate detection of features (James 1971). In 1975 La Violette and Hubertz managed to track packed ice motions successfully using AVHRR data. This opened the door to the use of AVHRR data as these proved relatively clear and had enhanced spatial and temporal resolutions (1km spatial and 24 hour temporal). Several studies since have been carried out using SST in AVHRR images including the determination of velocities related to cyclonic eddies (Spence and Legeckis 1981*;* Koblinsky et al. 1984) and the determination of surface velocities for the Oyashio Front near Hokkaido, Japan (Vastano and Bernstein 1984*;* Vastano and Borders 1984).

However, this method of manually tracking surface features is still regarded as being too subjective. Results would be unreliable as they are based on the choices made by the operator. It is also strenuous and labour intensive considering there are also other inaccuracies to manual tracking other than the advective assumption. Along-isotherm

and cross-isotherm SST components for example make it difficult to distinguish the motion of the flow. Selecting enough features to track and make a comprehensive determination of the flow can also prove challenging. Cloud cover is also a factor to consider as extensive cover may lead to insufficient features able to be tracked. Many of these limitations can be corrected to a certain degree by either carrying out cloud masking techniques or by reducing the time interval between images. The use of automatic, algorithmic feature-tracking techniques can also address some of these problems.

Maximum cross correlation

Cross-correlation, a form of objective statistical analysis, was first used in oceanography in the 1980's when investigations into appropriate correlation functions related to spatial variability were being conducted (Denman and Freeland, 1985). A study into the computation of ice motions by Ninnis et al. (1986) was also carried out using an automated tracking technique adapted from an earlier meteorological study by Leese et al. (1971). Emery et al. (1986) further developed this to track and depict oceanic meso-scale patterns from AVHRR data and referred to this method as maximum cross correlation (MCC). This method has since been used extensively to track meso-scale features and derive surface currents incorporating both AVHRR and CZCS data. Studies using MCC have been undertaken in the north-eastern Pacific (Tokmakian et al.1990*;* Kelly and Strub 1992*;* Crocker et al. 2007), the English Channel (Garcia and Robinson 1989), the north-western Pacific (Kamachi 1989), the north-western Atlantic (Emery, Fowler., 1992), the north-eastern Atlantic (Garcia Weil et al. 1994), east and west coast of the U.S. (Holland and Yan 1992) among other regions.

This tracking technique employs the use of subwindows in sequential images. The first subwindow, referred to as the template window, contains the features to be tracked. The subsequent image uses a search window inside which the template window from the previous image is searched for. The template window that correlates most (shows maximum correlation) with the first template window indicates the most likely displacement of said feature. The distance between the centre of the initial template window and the centre of the second template window can then be drawn and measured. This is then divided by the time separation between images to obtain a velocity vector. Template window size can vary depending on the feature to be tracked.

Studies using Sea Surface Temperature (SST) patterns as passive tracers tend to use template windows with sizes ranging from 20km-40km (Crocker et al.2007). If the template window is too small, the feature can be hard to search for in the subsequent image and the correlation coefficients will remain low (Notarstefano et al. 2007). However, if the template window is too large, the resulting vectors will be smoothed out spatially which can lead to inaccuracies. The size of the search window is dictated by the time separation between images as the window must be as large as the maximum displacement expected for the features. To ensure a better spatial resolution the search window can be overlapped, reducing the grid spacing (Ninnis et al.1986). This process when completed to its entirety (using all distinguishable features) can generate a velocity field representative of the surface current.

The MCC method although more objective, still contains sources of error related to those found in the manual tracking method. This includes the assumption that displacements are translational and negate rotational and deformational motions, although Kamachi (1989) modified the MCC to include rotational effects. With SST features in particular, the main source of error lies in the assumption that observable

displacements are solely due to advection. Undesirable viewing conditions and isothermal flow are also factors limiting the MCC method (Crocker et al.2007). Earth location accuracy must also be taken into account as navigational errors can reach magnitudes equivalent to the feature displacements themselves (Ktasnopolsky et al.1994). It was also found that velocities for areas of intense surface flow were underestimated by the MCC method (Kelly and Strub 1992). It should also be noted that the error analysis involved in evaluating the MCC technique has a certain degree of difficulty when carried out as the cross correlation brings with it an associated significance which is hard to deduce. This can usually arise due to ill-defined gradients (Breaker et al. 1994). Previous MCC evaluations have found that satellite derived velocities contain an rms error of 6cms^{-1} when compared to drifter derived flows and 14cms^{-1}-25cms^{-1} when compared to ADCP derived currents (Tokmakian et al.1990; Crocker et al. 2007).

The Benguela current

This study will focus on applying an MCC algorithm and derive velocities for the Benguela current at about 24^{o}S-28^{o}S and 9^{o}E-17^{o}E (Figure 1). This current receives flows from current rings emanating from the Algulhas Current at 40S 18E and becomes part of the South Atlantic current (Richardson P. L., and S.L., Garzoli 2003). The northward displacement of the Benguela current from the Alghulas is caused by the shelf positioned in the south-western region of Africa. This land mass causes the Benguela current to flow North to West whereby it is met by the Angola-Benguela Front travelling from the Equatorial Counter Current. With Africa bounding to the East, the current is pushed further West into the Atlantic. Current speeds during the summer months of June, July and August tend to vary between 7 and 17 cms^{-1} (Wedepohl et al., 2000; Shannon., 1985) The displacement resulting from the current is known to cause the upwelling of cold-nutrient rich water from the South Atlantic Intermediate water along the south-west coast of Africa (Shannon., 1985). Strong gradients in phytoplankton concentration or SST could potentially be utilised to derive the velocities in this region.

Methods

Data selection and manipulation

Chlorophyll-a was chosen to be the passive feature to be tracked as surface concentrations for this pigment in the Benguela region for July 2011 showed prominence (~ 6 – 13 mg m^{-3}). Two sequential colour images were provided by NASA's Ocean Color Browser (Figure 2). These were taken by the MODIS sensor on-board AQUA on July 14th 2011 at 13:10 GMT and July 15th 2011 at 12:15 GMT giving a time separation of 23 hours and 5 seconds. The spatial resolution associated to the band data is 1.1km. Level 0 to 2 processing had been previously carried out by The Ocean Biology Processing Group (OBPG). These processes include the removal of excess bands and the generation of geolocation files (Lvl-1A) as well as instrument calibration (Lvl-1B) and application of MODIS default chlorophyll-a algorithm (OC3; O'Reilly et al., 1998).

The images acquired were then navigated manually so as to position the images at the same geographical location. This was done by aligning the longitude and latitude coordinates of the four corner pixels in both images and cropping all the information

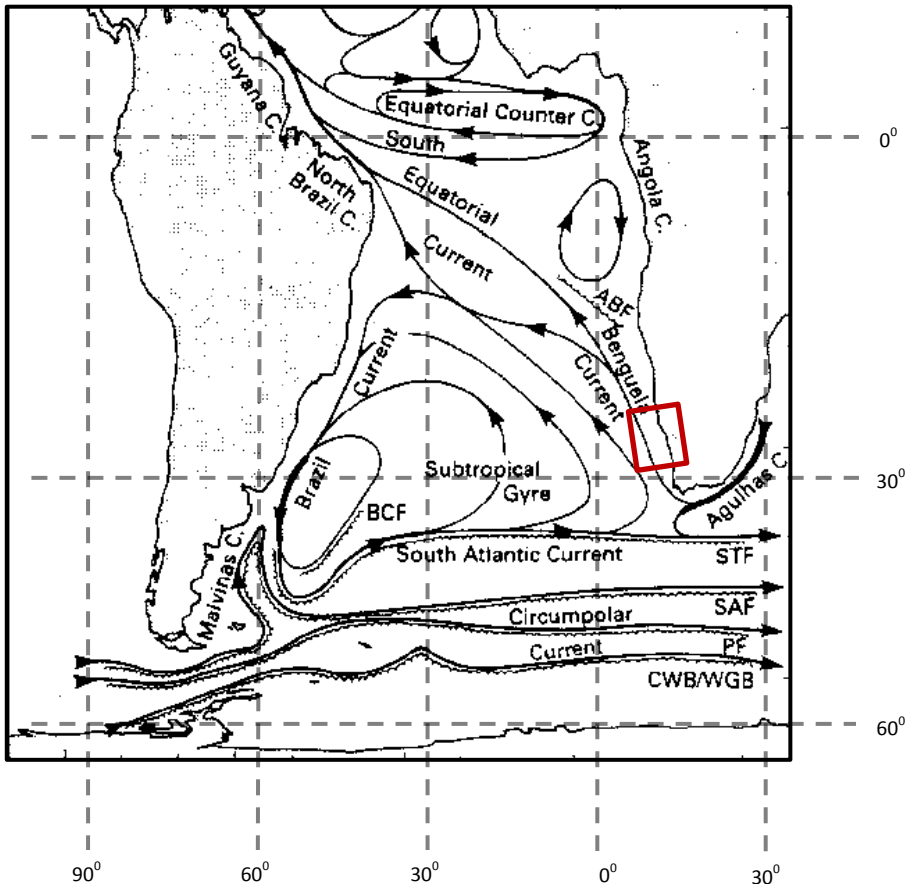

Figure 1: Surface Currents of the South Atlantic Ocean. Abbreviations used for Angola-Benguela Front (ABF), Brazil Current Front (BCF), Sub-tropical Front (STF), Sub-Antarctic Front (SAF), Polar Front (PF) and Continental Water Boundary / Wedell Gyre Boundary (CWB/WGB). Study area for this report is outlined by the red box. Image adapted from Tomczak and Godfrey (1994).

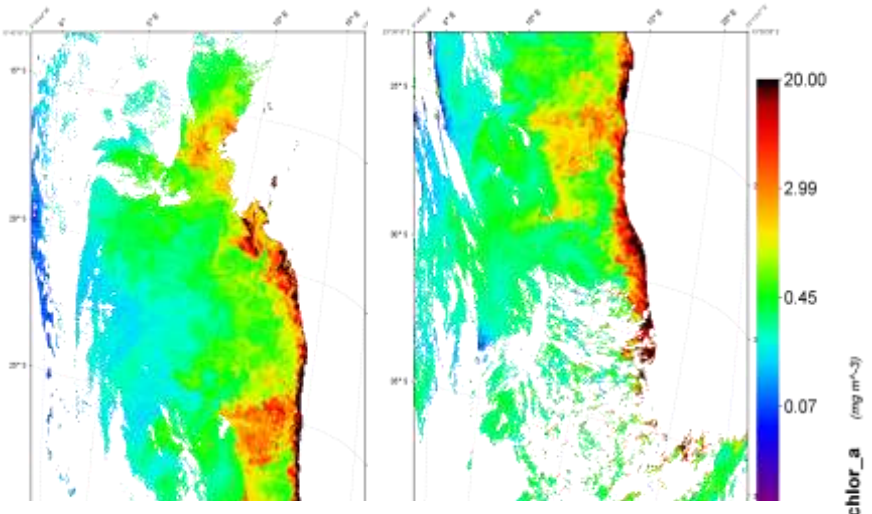

Figure 2: Colour images displaying chlorophyll-a concentration for Benguela region taken on July 14th 2011 at 13:10 GMT (Left) and July 15th 2011 at 12:15 GMT (Right). Images retrieved from *http://oceancolor.gsfc.nasa.gov/.*

external to this. The coordinates used were as follows: 24°10'11''S 9°38'16''E, 24°10'11''S 17°14'17''E, 28°33'39''S 9°38'16''E, 28°33'39''S 17°14'17''E. Figure 3 shows the navigated images ready for cross-correlation analysis.

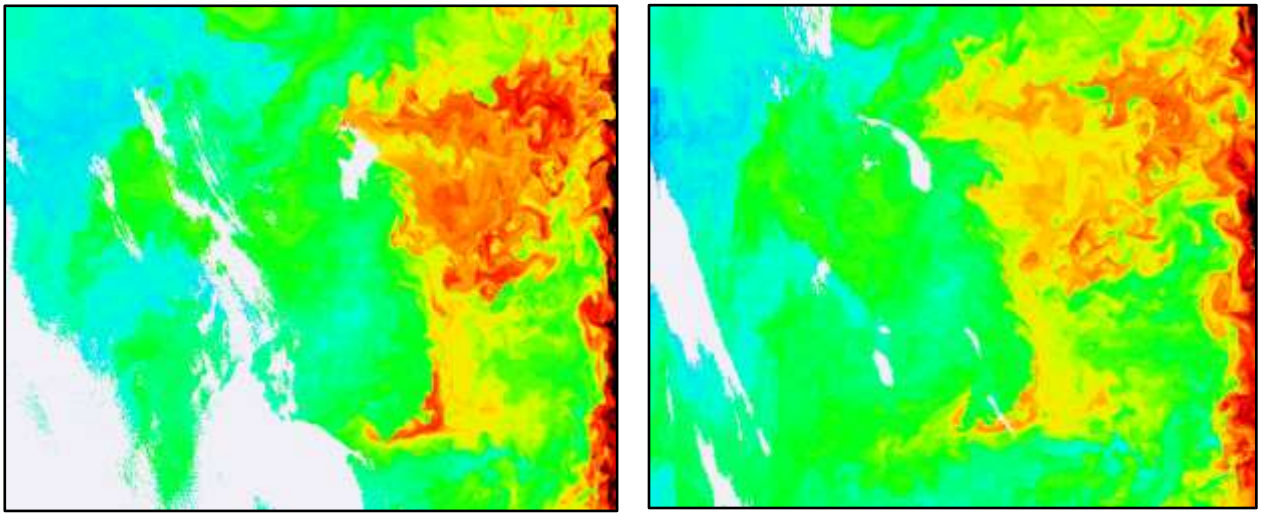

Figure 3: Navigated images showing chlorophyll feature to be tracked for image 1 (taken on the 14th) and image 2 (taken on the 15th).

Cross correlation analysis

Before applying the MCC analysis to the images prepared, certain parameters describing the statistical method needed to be set. Three scenarios using different values for subwindow size, search window size and correlation coefficient were used and the vector field outputs investigated. By subsequently comparing the resulting velocities with locally observed data, the scenario showing closest approximation to these could be identified and discussed. The values chosen can be seen in Table 1.

The processing algorithm used to compute the MCC begins by identifying feature positions using local maxima of the grey-scale variance. The variance is calculated for 5x5 pixel matrix regions. Subwindows with the centred features (positions of local maxima) are extracted from the first image and compared to a search window within the second image. The horizontal offset of features must lie within the search window limits so as to recognise the displacement. Comparisons with the subwindow from the initial image are made using normalised cross-correlation with a speed-accuracy trade-off.

Table 1: Three scenarios using different input values for subwindow and search window sizes as well as Convolution Tolerance (cross-correlation coefficient).

Run	Subwindow	Search window	Convolution Tolerance
A	21	100	0.1
B	41	150	0.5
C	61	200	0.8

This employs a convolution mask that approximates to the subwindow in the first image and rotates 180 degrees. A convolution tolerance parameter specifies the quality of the

approximation whereby the result is divided by the standard deviation of search regions in the second image. The maximum value in the search region is taken to show closest correlation (maximum cross-correlation) to the subwindow in the first image. Figure 4 displays the corresponding matches as optical flow vectors superimposed onto the second image for scenarios A, B and C.

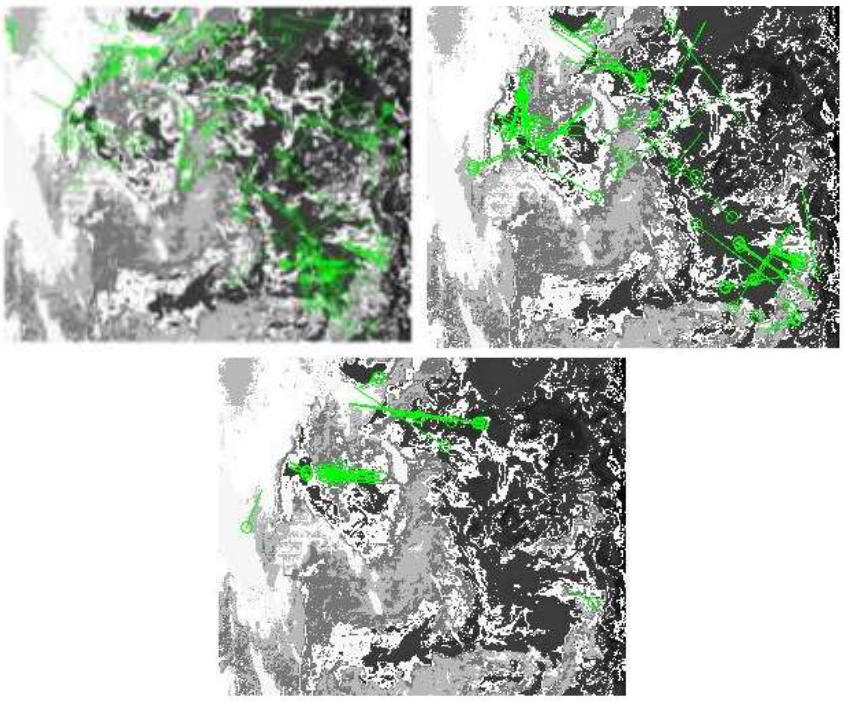

Figure 4: Optical flow vectors for runs A, B and C (left to right) displayed onto second image. Feature positions from the first image are shown by the green circles with the line pointing to the displaced position in the second image.

In-situ data

The data that was to be used to make a comparison with the velocities derived from the MCC method were collected and made freely available by the International Argo Program and the national programs that contribute to it. (http://www.argo.ucsd.edu, http://argo.jcommops.org). The Argo Program is part of the Global Ocean Observing System. Argo provides data taken from float drifters. Seven data sets containing drifter information were taken for July 10th to July 19th 2011 for the Benguela region between 24^{o} to 34^{o} S and 10^{o} to 14^{o} E. Velocities for the drifters could be subsequently derived from the displacements and trajectory periods. The resulting velocities can then be compared using statistical analysis of variances.

Results

Vector fields

The images displaying optical flow were further processed so as to represent the displacement vectors as u and v velocity products, the magnitude of which can be seen represented by the dark arrows seen in Figures 5, 6 and 7. The images were compared to altimetry plots using altimeter data produced by Salto/Duacs and distributed by Aviso, with support from Cnes (http://www.aviso.altimetry.fr/duacs/) (Figures 8 and 9.) The MCC field vectors agree with the orientation and magnitude of those in the altimeter

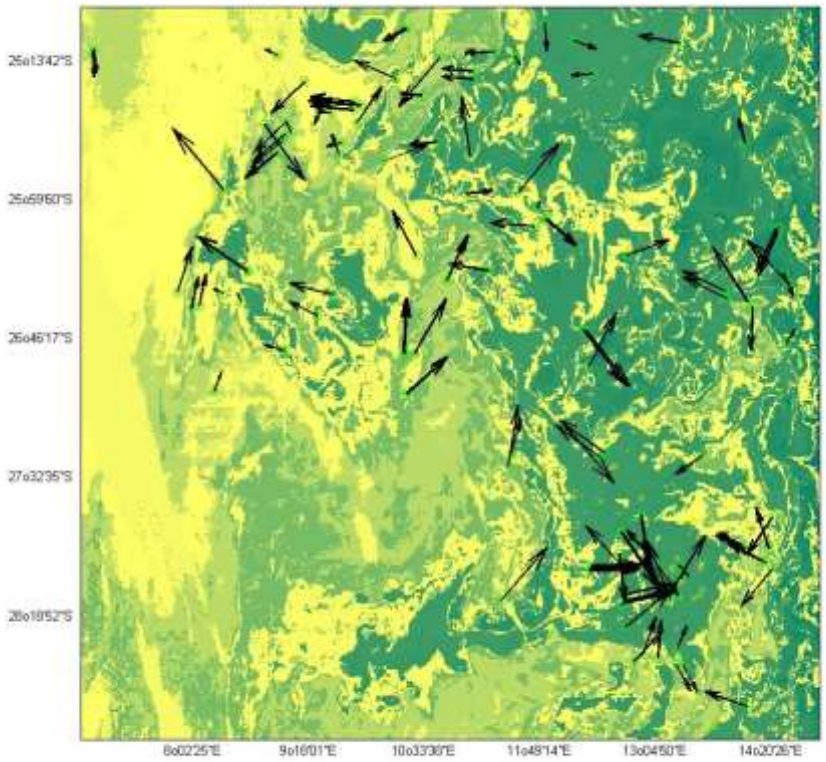

Figure 5: Velocity field output after MCC analysis using parameters specified for Run A in Table 1.

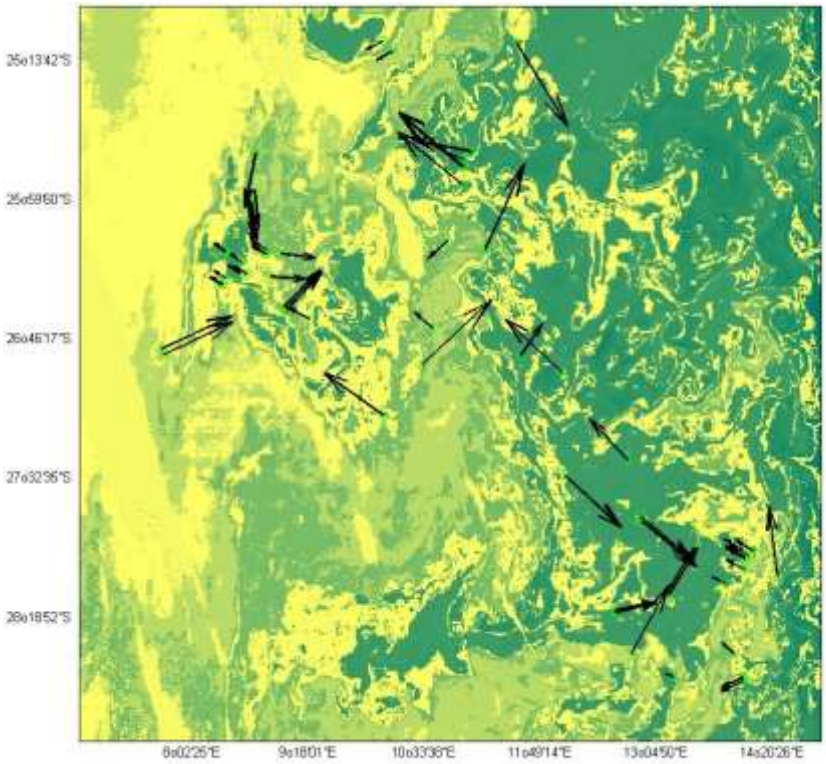

Figure 6: Velocity field output after MCC analysis using parameters specified for Run B in Table 1

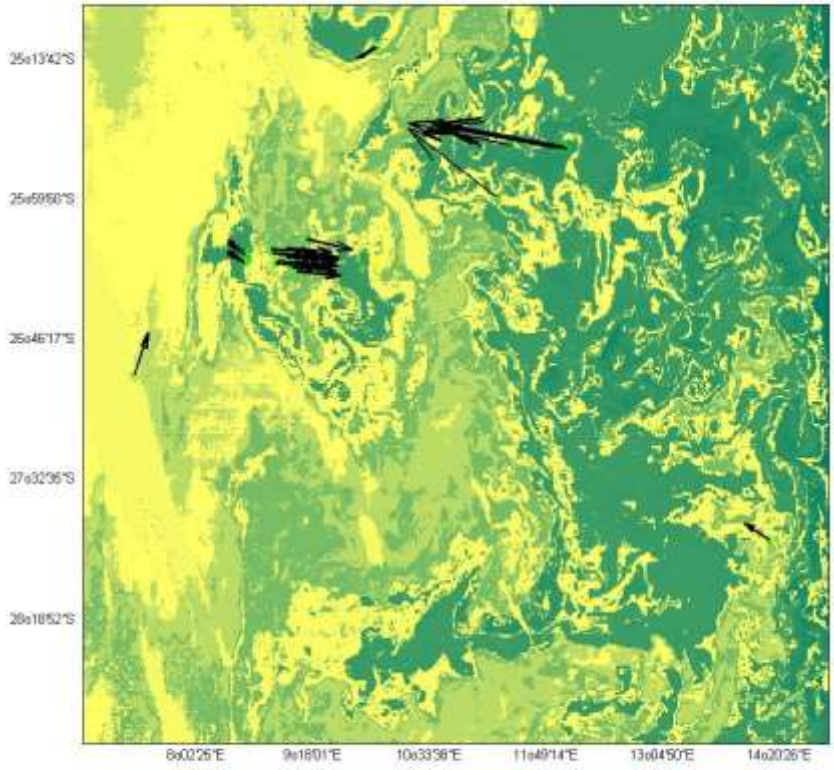

Figure 7: Velocity field output after MCC analysis using parameters specified for Run C in Table 1

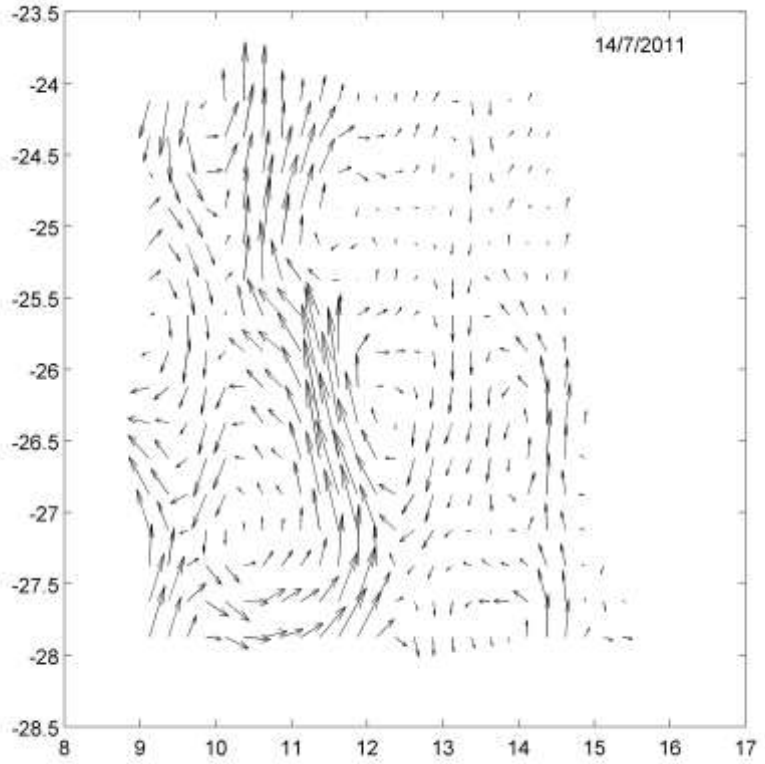

Figure 8: Velocity field derived using altimetry data provided by AVISO for 14th July 2011.

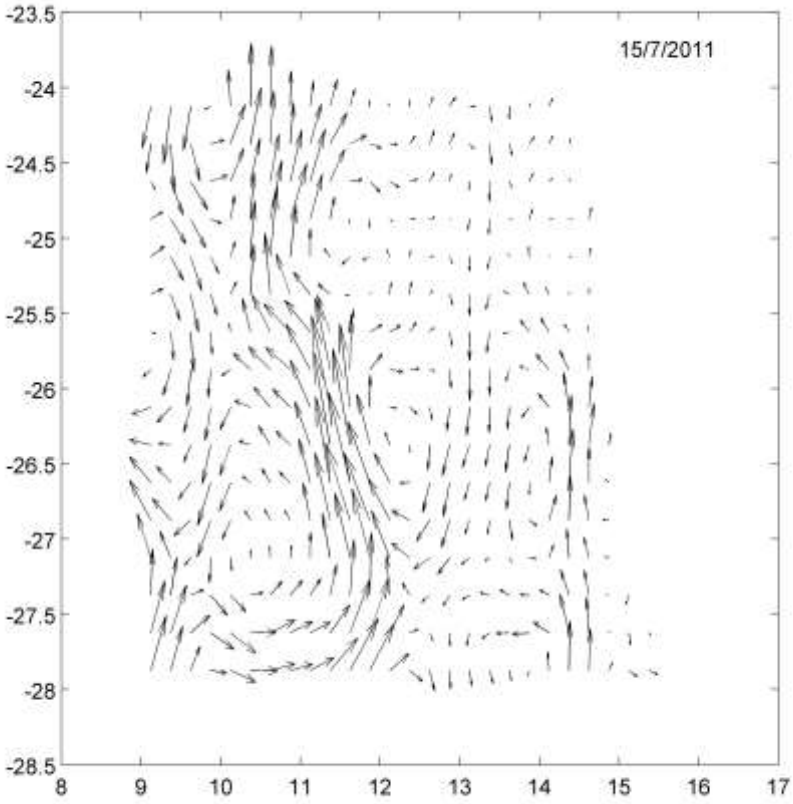

Figure 9: Velocity field derived using altimetry data provided by AVISO for 15th July 2011.

fields. Surface displacement for the gyre formation between 25.5°-26.5°S and 9.5°-11.5°E is evident in both the MCC and altimetry images. The altimetry data also show a noticeably strong current running South to North at 26.5°S 11.8°E. Traces of this pattern can be seen in Figure 5 and to an extent in Figure 6. This feature shows evidence of the Benguela current as, at certain locations, the current width spans almost 3° in longitude which is approximately 200 km. The Benguela current, as described by P.M. Wedepohl et al. (2000), has a width of 200 km towards the south (35°S) and up to 750 km in the Northern region (21°S). The draw of surface water moving away from the south-west coast of Africa (14.5°E) is driven by the south easterly-winds leaving the high pressure system in the central South Atlantic ocean gyre a travelling along the southern African coast (C.M.D. Rae, 2004). This explains the upwelling mechanism occurring in this region providing the distinguishable chlorophyll features used for tracking.

Surface velocities

The respective u and v components for the flow vectors were tabulated for each run as well as the mean u and v velocities and the total number of vectors produced for each field (Table 2). For the first scenario, (Run A; Figure 5), the cross-correlation was able to produce a total of 126 vectors. The absolute magnitudes (r.m.s) for the values were 10.55 cms^{-1} for u and 13.37 cms^{-1} for v. The r.m.s variability in u and v magnitudes was calculated to give 15.65 cms^{-1} and 64.30 cms^{-1} respectively. The second run (Run B; Figure 6) produced a velocity field displaying 70 vectors. The mean u and v velocity components for this run are 1.82 cms^{-1} and 15.97 cms^{-1} respectively. The r.m.s. variability associated to these velocities are of 189.15 cms^{-1} for u and 58.51 cms^{-1} for v. The mean and r.m.s variability of the velocity in the v direction is similar to that

Table 2: Tabulated results for three scenarios (Runs A, B and C).

Run	No Vectors	Max u (ms^{-1})	Max v (ms^{-1})	Mean u (ms^{-1})	Mean v (ms^{-1})	r.m.s u (ms^{-1})	r.m.s v (ms^{-1})
A	126	-1.27	-1.27	0.1055	0.1337	0.1565	0.6430
B	70	1.91	-1.91	0.0182	0.1597	1.8915	0.5851
C	29	-2.55	-1.17	0.1875	0.1212	0.4803	0.6109

computed for the first run which may suggest a common displacement of water away from the South-West coast of Africa and out into the South Atlantic. The u component however shows a much higher variability for the second run which may question the direction of the flow in terms of u. The final run (Run C; Figure 7) produced the field with fewest vectors. 29 velocities were displayed for this scenario which strongly suggests that the cross-correlation parameters have a large effect on the quantity of vectors produced. The mean values for the velocity components however are not too different from runs A and B. These were 18.75 cms^{-1} for u and 12.12 cms^{-1} for v. The respective r.m.s variability for run C was 48.03 cms^{-1} for u and 61.09 cm^{-1} for v. Again the variability in v follows that observed from previous runs. The u component for velocity however varies less than Run B and more than Run A.

The results for each velocity field were subsequently compared to the values derived from ARGO drifter trajectories (Table 3). An analysis of variance was conducted whereby the distribution of vector values from MCC and drifter derived velocities was tested against a significance level of 0.01. If the probability value (P) were to fall below this level, the hypothesis that the MCC derived values show the same distribution as those derived from the drifter buoys, could be made.

Table 3: Tabulated results from ARGO Drifter data. Δt denotes the trajectory period in seconds and ΔD the linear displacement.

ARGOS ID	Initial Latitude (degrees North)	Initial Longitude (degrees East)	Final Latitude (degrees North)	Final Longitude (degrees East)	Δt (s)	ΔD (m)	Mean V (m/s)
40746	-31.256	13.377	-31.251	13.337	22523	3844	0.17067
93926	-34.523	11.218	-34.606	11.119	27724	12941	0.46678
46440	-24.414	11.578	-24.376	11.619	34471	5926	0.171913
93927	-35.315	10.508	-35.291	10.337	26536	1575	0.059353
39931	-30.488	11.075	-30.474	11.065	41388	1829	0.044192
64146	-30.328	14.507	-30.281	14.488	41138	5537	0.134596
43944	-27.641	12.296	-27.621	12.294	21196	2233	0.10535

The P value calculated for Run A was 7.03×10^{-7}. This infers there is a 99% probability that both sets could be drawn from the same distribution. Run B can also be said to share a similar distribution as the P value for this case was 5.26×10^{-4}. The final run however gave a calculated P value of 0.0028. This is much higher than the other probability values and approximates closest to the significance level of 0.01. Despite this, the P value remains below the significance level and can therefore be said to show agreement with the value distribution representative of the drifter velocities.

Limitations

Aside from the mean velocity components, the results for each MCC run differ considerably. Specifically, the quantity of vector outputs seems to vary significantly with the first run producing the most and the final run producing the least. The selection of different cross-correlation parameters is the principal cause of this. Run A had a convolution tolerance of 0.1 which allows for an increased degree of flexibility when attempting to match similar features between images. As a consequence, the cross-correlation was able to identify more features than the following runs and draw displacements vectors between these. The low correlatory threshold however may cause the process to identify matches which are similar but not true to the exact feature located in the first image. This could lead to the drawing of erroneous vectors representative of false displacements. The size of the subwindow may also limit the identification of feature matches as features larger than 21 km would not be detected as they fall outside the window boundary. Similarly, the search window must be large enough to accommodate the largest expected displacement as vectors larger than this would fall outside of the window parameter and would not be recognised. To demonstrate the effects of this, the window size for both search and subwindows was increased. Figure 6 shows that new vectors had been identified that were larger than those observed in the first run. Figure 7 demonstrates this further with substantially larger displacements of fewer, larger features. The quantity of vectors produced from these runs however is much fewer with the third and final run displaying only 29. The reason for this decrease is likely due to the convolution tolerance parameter which was increased to 0.5 for Run B and 0.8 for Run C. This allows for ‘stricter’ feature matching as the values identified in the second images must fall closer to the value of the feature identified in the first image. Although fewer in number, the vectors produced after applying a higher tolerance are less likely to be erroneous due to the stricter conditions. From this process we can gather that the correlation parameters have a significant effect on the resulting field and should be set to values dependant on the local variations and size of the study region.

Aside from the potential limitations controlled by the cross-correlation parameters, a number of other factors could give rise to further inaccuracy. The time separation between images could severely limit the representation of the MCC field as the evolution of the complete current field may take much longer than 24 hours. Conversely, a surface displacement could occur and dissipate before the second image is able to detect it. A certain degree of error may also lie within the *in-situ* comparison as only seven drifter buoys were used making the analysis of variance less robust. The quality of the data may also lead to slight inaccuracies as, despite having undergone preliminary processing and calibration, the drifter equipment spends only ~10 hours at the surface before descending to a depth of ~1000m for 8-10 days. Although the data was only used for the first 10 hours, there was no way of assuring the buoy was consistently drifting along the surface. Another limitation may also stem from the human

error imposed by the operator during image manipulation as the navigational errors within the images may result in inaccurate vector representation.

Further measures can be taken to avoid these errors in future. The first improvement would be to use a much larger bank of *In-situ* data in order to make a more comprehensive statistical comparison. It may also be worth testing a much larger subset of correlation parameters individually to better observe how these vary the field output and select appropriate values that would best represent the local flow.

Conclusion

In conclusion the mean surface velocities derived using the MCC statistical method for the Benguela current region came into close approximation to those derived from ARGO drifters and values described in previous studies (Shannon 1985, Wedepohl et al. 2000). The vectors themselves were successful at demonstrating the magnitude and direction of individual displacements as these were compared to the fields represented by altimetry data. However due to statistical values defining the MCC method, too few vector outputs were computed and an accurate representation of the flow in its entirety could not be displayed. The scarce amount of local data may also have led to inaccuracies when making statistical evaluations. Physical processes within the region such as the upwelling of cold nutrient-rich water from the South Atlantic Intermediate waters are evident in the images by the displacements directed along the South African coast (bounding to the East of the fields) and by the increased surface chlorophyll concentrations.

Acknowledgments

I would like to thank Dr. Jill Schwarz for her continued support and guidance throughout this work. I would also like to acknowledge NASA, The Ocean Biology Processing Group and affiliates as well as the International Argo Program and the national programs that contribute to it. Also thank you to Ssalto/Duacs, Aviso and Cnes. Special thanks to Mathworks © and SeaDAS developers.

References

Barbanti, R., Lungwirth, R. and Poulain, P-M. (2005). Stime dell'accuratezza del drifter tipo CODE con GPS nella determinazione della posizione geografica. OGS Tech. Rep. 32/ 2005/OGA/20, 16 pp.

Barrick, D. E. (1977). Ocean surface currents mapped by radar. *Science*. 198 (4313), 1373-1375.

Bernstein, R. L.. (1982). Sea surface temperature estimation using NOAA 6 satellite advanced very high resolution radiometer. *Journal Geophysics Research*. 87 (12), 9455-9465.

Breaker, L. C. (1994). The feasibility of estimating ocean surface currents on an operational basis using satellite feature tracking methods. *Bulletin of the American Meteorological Society*. 75 (-), 2085-2095.

Bryden H. L. and Hall, M. M. (1980). Heat transport by currents across 25 N latitude in the Atlantic Ocean. . *Science*. 207 (-), 884-886

Burgess, F. J. and James, W. P. (1971). Air photo analysis of ocean outfall dispersion. *Federal Water Quality Office*. - (-), 290.

Crocker, I. R., Matthews, D.K. and Emery, W.J. (2007). Computing coastal ocean surface currents from infrared and ocean color satellite imagery. *Transactions on Geoscience and Remote sensing*. 45 (2), 435-447.

Denman, K. L. and Freeland, H. J. (1985). Correlation scales, objective mapping and a statistical test of geostrophy over continental shelf. *Journal of Marine Research*. 43 (23), 517-539.

Doty, R. (1958). Aloft with balloon and camera. *J. Photographs and motion pictures of George Eastman House*. 7 (-), 197-209.

Emery, W. J. and Fowler, C. W. (1991). Fram strait satellite image-derived ice motions. *Journal Geophysics Research*. 96 (3), 4751-4768.

Emery, W. J., Thomas, A.C., Collins, M.J., Crawford, W.R. and Mackas, D.L. (1986). An objective method for computing advective surface velocities from sequential infrared satellite images. *Journal Geophysics Research*. 91 (12), 865-878.

Garcia, C. A. E. and Robinson I. S. (1989). Sea surface velocities in shallow seas extracted from sequential Coastal Zone Color Scanner satellite data. *Journal Geophysics Research*. 94 (12), 681-691.

Garcia, W., Nykjaer L., Tejera-Cruz A., and Canton M. (1994). Cálculo de velocidades oceánicas superficiales en el área del afloramiento del NW de África mediante imágenes del sensor AVHRR, Rev. Asoc. Española de Teledetección, Nº 3, 37-41, 1994.

Goldstein, R. M. and Zebker, H. A.. (1987). Interferometric radar measurement of ocean surface currents. *Nature* . 328 (-), 707-709.

Holland, J. A. and Yan, X.H. (1992). Ocean thermal feature recognition, discrimination and tracking using infrared satellite imagery. *Transactions on Geoscience and Remote sensing*. 30 (10), 46-53.

James, W. P. (1972). Diffusion coefficients and current velocities in coastal waters by remote sensing techniques. *Remote Sensing of Environment*. 3 (-), 352-361.

Kamachi, M. (1989). Advective surface velocities derived from sequential images for rotational flow field: Limitations and applications of maximum cross-correlation method with rotational registration. *Journal Geophysics Research*. 94 (18), 227-233.

Kelly, K. A. and Strub, P.T. (1992). Comparison of velocity estimates from Advanced very high resolution radiometer in the coastal transition zone. *Journal Geophysics Research*. 97 (96), 53-68.

Koblinsky, C. J., Simpson, J. J. and Dickey, T. D. (1984). an offshore eddy in the California Current System. *Progr. Oceanogr.* 13 (-), 51-69.

Krasnoplosky, V. M. and Breaker, L.C. (1994). The problem of AVHRR image navigation revisited. *International Journal of Remote Sensing*. 15 (-), 979-1008.

La Violette, P. E. and Hubertz, J. M.. (1975). Surface circulation patterns of the east coast of Greenland as deduced from satellite photographs of ice floes. *Journal Geophysics Research*. 94 (-), 400-402.

Leese, J. A., Novak, C. S., Clarke, B. B.. (1971). An automated technique for obtaining cloud motion from geosynchronous satellite data using cross-correlations. *Journal of Application of Meteorology*. 10 (-), 118-132.

Notarstefano, G. Poulain, P. M. and Mauri, E.. (2007). Estimation of surface currents in the Adriatic sea from sequential infrared satellite images. *Journal of Atmospheric and Oceanic Technology*. 25 (2), 271-285.

Ninnis, R. M., Emery, W. J. and Collins, M. J. (1986). Automated extraction of pack ice motion from advanced very high resolution radiometer imagery. *Journal Geophysics Research*. 91 (10), 725-734.

Paduan, J. D. and Graber, H. C.. (1997). Introduction to high frequency radar. *Oceanography*. 10 (-), 36-39.

Richardson, P.L. and Garzoli, S.L. (2003). Characteristics of intermediate water flow in the Benguela current as measured with RAFOS floats. *Deep Sea Research*. 50 (2), 87-118.

Schmetz,J. and Nuret, M.. (1987). Automatic tracking of high-level clouds in Meteosat infrared images with a radiance windowing technique. *ESA*. 11 (-), 275-286.

Shannon, L.V. (1985). The Benguela Ecosystem, I., Evolution of the Benguela, physical features and processes. *Oceanography and Marine Biology*, 23, 105-182.

Spence, T. W. and Legeckis, R. (1981). Satellite and hydrographic observations of low-frequency wave motions associated with a cold core Gulf Stream ring. *Journal Geophysics Research*. 86 (-), 1945-1953.

Svejkovsky, J.. (1988). Sea surface flow estimation from advanced very high resolution radiometer and coastal zone color scanner satellite imagery: a verification study. *Journal Geophysics Research*. 93 (-), 6735-6743.

Tokmakian, R., Strub, P. T. and Mclean-Padman, J.. (1990). Evaluation of the maximum cross-correlation method of estimating sea surface velocities from sequential satellite images. *Journal of Atmospheric and Oceanic Technology*. 7 (-), 852-865.

Tomczak, M., and Godfrey, J.S. (1994). *Regional oceanography: an introduction*, p422, Pergamon, New York.

Vastano, A. C. and Bernstein, R. L. (1984). Mesoscale features along the First Oyashio intrusion. *Journal Geophysics Research*. 89 (-), 587-596.

Vastano, A. C. and Borders, S. E. (1984). Sea surface motion over an anticyclonic eddy on the Oyashio Front. *Remote Sensing of Environment*. 16 (-), 87-90.

Wedepohl, P.M., Lutjeharms, J.R.E. and Meeuwis, M. (2000). Surface drift in the south-east Atlantic ocean. *South African journal of Marine Science*. 22 (1), 71-79.